THE LUMINOSITY FUNCTION OF QSO HOST GALAXIES

Timothy S. Hamilton,[1,2,3] Stefano Casertano,[2] and David A. Turnshek[1]

ABSTRACT

We present some results from our *HST* archival image study of 71 QSO host galaxies. The objects are selected to have $z \leq 0.46$ and total absolute magnitude $M_V \leq -23$ in our adopted cosmology ($H_0 = 50$ km s^{-1} Mpc^{-1}, $q_0 = 0.5$, and $\Lambda = 0$). The aim of this initial study is to investigate the composition of the sample with respect to host morphology and radio loudness, as well as to derive the QSO host galaxy luminosity function. We have analyzed available WFPC2 images in R or I band (U band, in one case), using a uniform set of procedures. The host galaxies span a narrow range of luminosities and are exceptionally bright, much more so than normal galaxies, usually $L > L_V^*$. The QSOs are almost equally divided among three subclasses: radio-loud QSOs with elliptical hosts, radio-quiet QSOs with elliptical hosts, and radio-quiet QSOs with spiral hosts. Radio-loud QSOs with spiral hosts are extremely rare. Using a weighting procedure, we derive the combined luminosity function of QSO host galaxies. We find that the luminosity function of QSO hosts differs in shape from that of normal galaxies but that they coincide at the highest luminosities. The ratio of the number of quasar hosts to the number of normal galaxies at a luminosity L_V is $\mathscr{R} = \left(L_V/11.48 L_V^* \right)^{2.46}$, where L_V^* corresponds to $M_V^* = -22.35$, and a QSO is defined to be an object with total nuclear plus host light $M_V \leq -23$. This ratio can be interpreted as the probability that a galaxy with luminosity L_V will host a QSO at redshift $z \approx 0.26$.

Subject headings: galaxies: elliptical and lenticular, cD — galaxies: spiral — quasars: general

1. INTRODUCTION

Much has been learned about the properties of QSO host galaxies since they were first imaged almost three decades ago (Kristian 1973). Early results include establishing a positive correlation between host and nuclear QSO luminosities (Hutchings, Crampton, & Campbell 1984) and indications of a morphological difference between radio-loud and radio-quiet QSOs, with the former more likely to be in elliptical hosts and the latter in spiral hosts (Malkan, Margon, & Chanan 1984). Boroson, Persson, & Oke (1985), as well as Stockton & MacKenty (1987), examine hosts to classify them spectroscopically and in the context of their nuclear emissions. Working in the near-infrared, where the luminosity contrast is more favorable to the host galaxy, Dunlop et al. (1993) show that QSO hosts are typically drawn from the bright end of the galaxy luminosity function (in agreement with Hutchings et al. 1984). McLeod & Rieke (1994a, 1994b), also using near-infrared data, find that hosts of radio-quiet QSOs are typically represented by an exponential (spiral disk) light profile (in agreement with Malkan et al. 1984) and that high-luminosity QSOs generally have brighter hosts than low-luminosity QSOs (in agreement with Hutchings et al. 1984).

High-resolution space-based images taken with the *Hubble Space Telescope* (*HST*) make observing the host galaxies much easier. The first, and to date one of the largest, systematic *HST* study of QSO hosts is by Bahcall et al. (1997), who study 20 of the most luminous nearby QSOs.

They can discern the morphology of the hosts, and they discover that, while radio-loud QSOs are found only in ellipticals or interacting systems, radio-quiet QSOs can be in ellipticals, spirals, or interacting systems. They also find that QSO hosts do not follow a Schechter (1976) luminosity function and are instead found at systematically high luminosities. More recent studies strengthen and expand on these results. McLure et al. (1999) confirm that QSO hosts are generally luminous and also determine that, even for radio-quiet QSOs, the hosts are often ellipticals or bulge-dominated. Furthermore, elliptical hosts appear to follow the same luminosity–surface brightness relation as field elliptical galaxies (Hamabe & Kormendy 1987). Other recent studies include Nolan et al. (2001), who discuss QSO host ages, and Kukula et al. (2001), who study host evolution from redshifts of $z \approx 2$ to the local universe.

In this paper, we focus on the luminosity distribution of a large sample of QSO hosts observed with the Wide Field Planetary Camera 2 (WFPC2) aboard *HST* (§ 2). We have collected and reanalyzed wideband archival images of 71 QSOs with $M_V \leq -23$ mag (total nuclear plus host light) and redshifts $0.06 \leq z \leq 0.46$. We have taken an inclusive approach in our sample selection, imposing no additional selection criteria on the QSOs besides those of total absolute magnitude and redshift, while some of the previous work on QSO hosts has focused on specific classes of QSOs: radio-loud (Lehnert et al. 1999), intrinsically very bright (Bahcall et al. 1997), and so on. For each QSO, we have subtracted the nuclear light component, using two-dimensional image fits, and have derived the luminosity and size of the underlying host galaxy by fitting both an $r^{1/4}$ and an exponential light profile (§ 3). Given the total number of objects considered, more than triple that of previous studies, we can effectively sample the general QSO population for redshifts $z \leq 0.46$ and derive a global luminosity function for their host galaxies that is not grossly affected by selection criteria

[1] Department of Physics and Astronomy, University of Pittsburgh, Pittsburgh, PA 15260; turnshek@pitt.edu.

[2] Space Telescope Science Institute, 3700 San Martin Drive, Baltimore, MD 21218; stefano@stsci.edu.

[3] Present address: Code 662, NASA/GSFC, Greenbelt, MD 20771; hamilton@milkyway.gsfc.nasa.gov.

(§ 4). This luminosity function is compared with that of normal galaxies, and selection effects/biases and other issues are discussed (§ 5). Conclusions are then summarized (§ 6).

Throughout this paper, we adopt a Friedmann cosmology with $H_0 = 50$ km s^{-1} Mpc^{-1}, $q_0 = 0.5$, and $\Lambda = 0$. We have converted the results of other researchers to this cosmology when comparing our results with theirs.

We confirm previous results that host galaxies of QSOs are significantly more luminous than typical luminous L_V^* galaxies, where L_V^* is the "knee" in the Schechter (1976) luminosity function. We also consider the relationship between host morphology and QSO radio loudness. Spiral hosts are, on average, nearly as luminous as elliptical hosts, while hosts of radio-loud QSOs are, on average, about 0.5 mag brighter than hosts of radio-quiet QSOs. Subject to systematic uncertainties in normalization procedures, we find that the combined low-redshift QSO host luminosity function has a very different shape from that of normal galaxies but that they coincide at the highest luminosities. In approximate terms, at redshift $z \approx 0.26$ the ratio of the number of these QSO hosts to the number of normal galaxies of luminosity L_V is $\mathscr{R} \approx (L_V/11.48L_V^*)^{2.46}$, where L_V^* corresponds to $M_V^* = -22.35$.

2. SAMPLE SELECTION

Our sample includes 71 QSOs with total magnitudes $M_V \leq -23$, redshifts $0.06 \leq z \leq 0.46$, and available WFPC2 observations in wideband filters. The objects are listed in Table 1, along with the HST programs under which they were obtained. The median redshift of this sample is $z = 0.24$, close to the midpoint of the range considered. The two-thirds of the sample surrounding the median point falls within the range $0.14 \leq z \leq 0.41$. We have analyzed or reanalyzed HST archival imaging observations in a systematic and uniform manner, and the results are reported in Table 1. Comparisons are made between the magnitudes we determine and the results of the original observers in § 5.4. The absolute magnitude selection ($M_V \leq -23$) aims at including only historically traditional QSOs. However, since the selection is based on the combined magnitude of the host and nucleus, lower luminosity nuclei, down to $M_V \approx -19$, are in fact included in our sample. We have not excluded these objects from our analysis, since they would be present in most magnitude-selected, ground-based samples.

We limit our analysis to objects with $z \leq 0.46$, in order to obtain a significant sample size and to ensure that the HST resolution permits a reasonably reliable separation between host and nuclear components. At $z \approx 0.4$, a typical host with a half-light radius of 9 kpc has an apparent radius of $1''.4$, which corresponds to 14 pixels in the Wide-Field Camera (WFC), or 31 pixels in the Planetary Camera (PC). The light from a luminous host should therefore be clearly separated from that of the nucleus. In fact, the host galaxy cannot be convincingly detected in only one of the 71 QSOs in our sample; this one is listed as such in Table 1.

Radio loudness data are collected primarily from Brinkmann, Yuan, & Siebert (1997) and Yuan et al. (1998), both of whom use a loudness criterion that classifies an object as radio-loud if it has a radio-to-optical flux density ratio in excess of 10. Radio loudness data for the remaining objects come from a variety of sources, with extensive use made of the NASA Extragalactic Database (NED).

3. MEASUREMENT TECHNIQUE

Even at HST resolution, the light of the unresolved nuclear central source significantly affects the extended light distribution of the host galaxy. A careful subtraction of the central point source is needed in order to measure the properties of the host accurately. The following is a brief description of our technique, which is largely similar to that of Remy et al. (1997).

Because of the complex structure of the HST WFPC2 point-spread function (PSF), our analysis procedure has three principal steps. (1) A model of the PSF is fitted to the central point source, in order to determine its subpixel position and the telescope focus, which affects the shape of the PSF. (2) The PSF and a galaxy model are simultaneously fitted to the entire image, to distinguish the nuclear and host components. (3) The nuclear magnitude is determined from the PSF model. Then the fitted PSF is subtracted, and the magnitude of the host is determined from the residual light.

The fitting of a model PSF, as opposed to an observed PSF, is dictated by both opportunity and quality considerations. Since we rely on archival data, in most cases we do not have a PSF observation taken at the same time as the QSO image. The PSF in WFPC2 varies with time as a consequence of short- and long-term changes in the telescope focus. Thus, using a PSF observed at other times does not generally yield a good subtraction of the nuclear light. Also, the undersampled nature of WFPC2 images make PSF subtraction very difficult, unless both PSF and image have been properly dithered. Under these circumstances, a cleaner PSF subtraction can be achieved by using a model PSF produced by the Tiny Tim software (Krist & Burrows 1995), provided that both focus and subpixel positions are explicitly fitted (Remy et al. 1997; Surdej et al. 1997). This also results in photometry that is comparable in accuracy to using an observed PSF.

3.1. First Step: Fitting the PSF

The model PSF is constructed from a set of artificial PSFs created using the Tiny Tim software (Krist & Hook 2001).[4] Tiny Tim uses a detailed model of the telescope and camera optics, including the zonal errors in the primary and secondary mirrors, to produce a good, wavelength-dependent approximation of the resulting PSF. However, the PSF structure changes significantly depending both on the telescope focus and on exactly how the point source is centered with respect to the pixel grid. The telescope focus changes with time as a result of "breathing," which is the thermal expansion and contraction of the spacecraft due to changes in its attitude relative to the Sun. Breathing typically changes the relative positions of the primary and secondary mirrors by about 5 μm.

Therefore, we produce PSF models oversampled 11 times, i.e., on virtual pixels 11 times smaller in area than actual detector pixels, and for focus positions that range from -10 to $+10$ μm in 1 μm steps. Each PSF is then aligned with various offsets with respect to the true pixel grid and resampled to the actual detector resolution, including the estimated pixel spread function described in the Tiny Tim documentation. The best fit to the light distribution in the central few pixels identifies the subpixel position and the

---

[4] Available at http://www.stsci.edu/software/tinytim/tinytim.pdf.

TABLE 1
OBSERVATIONS AND DATA

R.A. (J2000.0) (1)	Decl. (J2000.0) (2)	Name (3)	z (4)	CCD (5)	Filter (6)	$t_{\rm exp}$ (s) (7)	$m_{\rm nuc}$ (8)	$m_{\rm host}$ (9)	M_V(nuc) (10)	M_V(host) (11)	Morphology (12)	Radio Loudness (13)	Program (14)
00 23 11.1	+00 35 16.5	LBQS 0020+0018	0.423	PC1	F675W	1200	19.30	19.34	−22.45	−22.77	E	Q	5450
00 24 03.7	−02 45 27.8	LBQS 0021−0301	0.422	PC1	F675W	1200	19.03	19.10	−22.74	−23.03	E	Q	5450
00 24 32.5	−29 28 55.5	MRC 0022−297 [a]	0.406	PC1	F336W	2100	. . .	. . .	. . .	. . .	. . .	L	5974
00 45 46.6	+04 11 15.8	PG 0043+039	0.385	PC1	F702W	1800	16.04	19.03	−25.49	−22.67	E	Q	6303
00 54 55.7	+25 25 47.2	PG 0052+251	0.155	WF3	F606W	2100	16.04	16.83	−23.80	−23.08	S	Q	5343
00 57 11.6	+14 45 24.5	PHL 909	0.171	WF3	F606W	2100	15.97	16.89	−24.07	−23.29	E	Q	5343
01 03 13.0	+02 21 10.5	UM 301	0.393	PC1	F675W	1280	17.66	19.44	−23.92	−22.44	E	Q	5450
01 36 22.4	+20 57 14.7	3C 47	0.425	PC1	F702W	280	17.82	18.75	−24.07	−23.37	E	L	5476
01 37 39.0	+33 09 22.0	3C 48	0.367	PC1	F814W	3500	15.74	16.18	−25.72	−24.83	EI	L	5235
01 39 59.0	+01 31 01.6	PHL 1093	0.26	WF2	F675W	1871	17.21	17.17	−23.47	−23.54	E	L	6776
01 59 52.2	+00 23 50.1	Mrk 1014	0.163	PC1	F814W	480	16.17	14.75	−23.30	−24.34	S	Q	5982
02 02 05.1	−76 20 04.3	PKS 0202−76	0.389	PC1	F702W	1800	16.67	18.72	−24.98	−23.12	E	L	6303
02 07 49.5	+02 43 43.0	NAB 0205+02	0.155	WF3	F606W	2100	15.40	18.08	−24.37	−21.77	S	Q	5343
02 47 42.2	+19 40 09.4	Q0244+194	0.176	WF2	F675W	1871	16.80	17.54	−23.29	−22.47	E	Q	6776
03 00 31.6	+02 40 06.7	US 3498	0.115	WF2	F675W	1871	19.30	15.87	−19.79	−23.10	S	Q	6776
03 11 46.7	−76 51 40.8	PKS 0312−77	0.223	PC1	F702W	1800	16.13	16.67	−24.40	−23.78	E	L	6303
03 18 07.9	−34 25 52.2	Q0316−346	0.260	WF3	F606W	2100	16.21	18.08	−24.68	−23.03	IS	Q	5343
03 43 30.0	+04 57 48.6	3C 93	0.357	PC1	F702W	280	18.58	18.49	−23.51	−23.73	E	L	5476
04 52 32.4	−29 53 41.0	IR 0450−2958	0.286	PC1	F702W	1800	15.40	17.17	−25.41	−23.65	SI	Q	6303
07 39 18.0	+01 37 04.6	PKS 0736+01	0.191	WF2	F675W	1871	16.30	16.70	−24.03	−23.58	E	L	6776
07 57 57.8	+39 20 34.7	MS 07546+3928	0.096	PC1	F814W	610	14.26	14.37	−24.22	−23.47	E	Q	6361
08 04 35.3	+64 59 53.9	IR 0759+6508	0.149	PC1	F702W	1800	15.94	15.65	−23.57	−23.73	SI	Q	6303
08 04 55.0	+21 20 45.7	MS 0801.9+2129	0.118	PC1	F814W	610	16.00	15.66	−22.91	−22.80	S	Q	6361
08 39 52.6	−12 14 42.7	3C 206	0.198	PC1	F702W	600	16.07	16.90	−24.03	−23.09	E	L	5957
09 06 31.9	+16 46 11.5	3C 215	0.412	PC1	F814W	5000	17.71	18.23	−24.08	−23.08	E	L	5988
09 25 57.7	+19 53 45.4	PG 0923+201	0.19	WF3	F606W	2100	15.53	17.46	−24.73	−23.00	E	Q	5343
09 46 50.7	+13 19 52.6	MS 0944.1+1333	0.131	PC1	F814W	600	14.89	15.93	−24.16	−22.52	E	Q	6361
09 56 48.7	+41 15 47.2	PG 0953+414	0.234	WF2	F675W	1991	15.17	17.21	−25.23	−23.22	S	Q	6776
10 04 00.4	+28 55 20.2	PG 1001+291	0.330	WF3	F702W	2400	15.59	17.90	−25.58	−23.33	S	Q	5949
10 07 29.1	+12 48 33.3	PKS 1004+13	0.24	WF3	F606W	2100	15.15	17.00	−25.62	−24.06	E	L	5343
10 14 56.2	+00 34 21.2	PG 1012+008	0.185	WF2	F675W	1931	16.22	16.76	−23.75	−23.19	SI	Q	6776
10 31 52.5	−14 16 10.9	He 1029−1401	0.086	WF3	F606W	2100	13.84	15.86	−24.79	−22.74	E	Q	5343
11 02 38.2	+72 46 09.9	MS 1059.0+7302	0.089	PC1	F814W	600	16.60	15.41	−21.65	−22.34	S	Q	6361
11 19 06.7	+21 18 39.3	PG 1116+215	0.177	WF3	F606W	1800	14.85	16.74	−25.19	−23.42	S	Q	5099
12 04 42.2	+27 54 12.0	PG 1202+281	0.165	WF3	F606W	1800	16.85	17.39	−23.03	−22.62	E	Q	5099
12 12 27.9	+12 42 54.5	LBQS 1209+1259	0.418	PC1	F675W	1200	19.35	19.38	−22.39	−22.71	E	Q	5450
12 19 23.1	+06 38 26.8	PG 1216+069	0.331	PC1	F702W	1800	15.42	18.70	−25.76	−22.55	E	Q	5143
12 20 37.2	+17 18 24.4	LBQS 1218+1734	0.444	PC1	F675W	1200	18.33	19.01	−23.54	−23.26	E	L	5450
12 21 45.9	+75 19 06.5	MS 1219.6+7535	0.071	PC1	F814W	610	15.06	14.56	−22.72	−22.52	ED	Q	6361
12 25 10.7	+09 54 38.8	LBQS 1222+1010	0.398	PC1	F675W	1200	18.38	18.62	−23.23	−23.24	S	Q	5450
12 25 15.0	+12 18 40.2	LBQS 1222+1235	0.412	PC1	F675W	1200	17.68	18.25	−24.04	−23.82	E	L	5450
12 29 09.9	+02 03 02.3	3C 273	0.158	WF3	F606W	1800	12.60	15.65	−27.19	−24.24	E	L	5099
12 32 03.6	+20 09 29.2	PG 1229+204	0.064	PC1	F702W	560	15.37	15.04	−22.27	−22.33	S	Q	5502
12 42 39.5	+17 38 22.6	LBQS 1240+1754	0.458	PC1	F675W	1480	17.98	19.31	−23.93	−23.02	E	Q	5450
12 46 30.2	+16 45 23.5	LBQS 1243+1701	0.459	PC1	F675W	1400	18.45	18.44	−23.49	−23.91	E	Q	5450
12 52 25.2	+56 34 36.4	3C 277.1	0.321	PC1	F702W	280	17.97	18.35	−23.09	−22.76	S	L	5476
13 05 36.1	−10 33 36.2	PG 1302−102	0.278	WF3	F606W	1800	15.19	17.35	−25.93	−24.14	E	L	5099
13 09 47.0	+08 19 49.5	PG 1307+085	0.155	WF3	F606W	1800	15.46	17.47	−24.33	−22.42	E	Q	5343
13 12 16.3	+35 14 36.7	PG 1309+355	0.184	WF3	F606W	2100	15.56	16.61	−24.53	−23.62	S	L	5343
14 00 33.9	+04 04 46.8	PG 1358+04	0.427	PC1	F702W	1800	15.96	18.02	−25.84	−24.02	E	Q	6303
14 04 38.7	+43 27 07.5	Q1402+436	0.323	PC1	F702W	560	15.15	17.42	−25.93	−23.73	EI	Q	5178
14 05 12.9	+25 55 17.7	PG 1402+261	0.164	WF3	F606W	2100	15.73	17.33	−24.12	−22.62	S	Q	5343
14 19 05.7	−13 10 56.5	MS 1416.3−1257	0.129	PC1	F814W	600	15.83	16.90	−23.37	−21.70	E	Q	6361
14 27 33.6	+26 32 52.9	B2 1425+267	0.366	WF3	F814W	3500	15.88	17.47	−25.49	−23.45	E	L	5235
14 29 08.6	+01 17 13.0	MS 1426.5+0130	0.086	PC1	F814W	610	14.30	14.49	−23.87	−23.17	S	Q	6361
14 46 49.1	+40 34 34.7	PG 1444+407	0.267	WF3	F606W	2326	15.80	17.37	−25.14	−23.81	S	Q	5849
15 14 39.2	+36 50 37.7	B2 1512+37	0.371	WF3	F814W	1600	16.04	17.31	−25.38	−23.66	E	L	6490
15 22 30.7	−06 44 43.1	MS 1519.8−0633	0.083	PC1	F814W	600	16.01	15.07	−22.32	−22.75	S	Q	6361
15 47 47.5	+20 51 33.1	3C 323.1	0.264	WF3	F606W	1800	16.07	18.01	−24.94	−23.33	E	L	5099
15 50 42.5	+11 19 54.2	MC 1548+114A	0.436	WF3	F702W	1400	18.27	19.92	−23.66	−22.20	SI	L	5682
16 37 46.5	+11 49 49.7	MC 1635+119	0.146	WF2	F675W	1931	18.12	16.73	−21.38	−22.62	E	Q	6776
17 04 38.3	+60 44 51.4	3C 351	0.372	PC1	F702W	1800	15.50	16.97	−25.96	−24.59	S	L	6303
21 37 48.1	−14 32 30.9	PKS 2135−147	0.200	WF2	F675W	1931	16.21	16.91	−23.96	−23.23	E	L	6776

TABLE 1—*Continued*

R.A. (J2000.0) (1)	Decl. (J2000.0) (2)	Name (3)	z (4)	CCD (5)	Filter (6)	t_{exp} (s) (7)	m_{nuc} (8)	m_{host} (9)	M_V(nuc) (10)	M_V(host) (11)	Morphology (12)	Radio Loudness (13)	Program (14)
21 43 38.3	+17 43 14.2	OX 169	0.211	WF2	F675W	1871	15.89	17.28	−24.59	−23.18	EI	L	6776
22 02 56.6	−56 59 10.7	MS 2159.5−5713	0.083	PC1	F814W	610	17.14	15.01	−20.91	−22.52	S	?	6361
22 03 15.0	+31 45 38.3	Q2201+315	0.295	PC1	F702W	560	15.46	16.75	−25.78	−24.50	E	L	5178
22 16 51.7	−18 48 14.0	LBQS 2214−1903	0.396	PC1	F675W	1280	18.81	19.27	−22.81	−22.60	S	Q	5450
22 17 45.8	−03 32 47.1	Q2215−037	0.242	PC1	F702W	1800	18.69	17.38	−22.06	−23.29	E	Q	5143
22 50 27.5	+14 19 09.7	PKS 2247+14	0.237	WF2	F675W	1871	16.65	17.22	−23.90	−23.32	E	L	6776
23 47 27.6	+18 44 06.9	Q2344+184	0.138	WF2	F675W	1871	20.22	16.68	−19.16	−22.60	S	Q	6776
23 51 53.0	−01 09 27.8	PKS 2349−014	0.174	WF2	F675W	1871	15.97	15.63	−23.82	−24.07	IE	L	6776

Notes.—Units of right ascension are hours, minutes, and seconds, and units of declination are degrees, arcminutes, and arcseconds. Col. (7): Exposure time. Col. (8): Apparent nuclear magnitude in filter. Col. (9): Apparent host magnitude in filter. Col. (10): Absolute V nuclear magnitude. Col. (11): Absolute V host magnitude. Col. (12): Host morphology: E, elliptical; S, spiral; EI, elliptical undergoing strong interaction; SI, spiral undergoing strong interaction; ED, elliptical with possible inner disk; IE, irregular or interacting that is best fitted with an elliptical model; IS, irregular or interacting that is best fitted with a spiral model. Col. (13): Radio loudness: Q, radio-quiet; L, radio-loud; ?, not available. Col. (14): Observing programs and principal investigators: 5099, Bahcall; 5143, Macchetto; 5178, Hutchings; 5235, Westphal; 5343, Bahcall; 5450, Impey; 5476, Sparks; 5502, Sparks; 5682, Burbidge; 5849, Bahcall; 5949, Lanzetta; 5957, Sparks; 5974, Lehnert; 5982, Sanders; 5988, Ellingson; 6303, Disney; 6361, Boyle; 6490, Stockton; 6776, Dunlop.

[a] Host not detected.

estimated focus of the observation. If the PSF is not saturated, we can achieve a precision of ≈0.01 pixels in the central position and ≈1 μm in the focus position for QSOs dominated by their nuclei. During this procedure, the light of the extended galaxy, which varies little over the scale of the PSF, is treated as a constant background.

In some cases, several of the pixels at the core are overexposed and saturated on the CCD. These pixels provide no information and are masked from all fits. The pixels vertically adjacent to them are also masked, because the CCD "blooming" effect could have altered those pixels' intensity values. Our technique works in the presence of saturation, although the focus position is determined less accurately. Most images have either no saturation or a small amount that does not completely cover the PSF core.

Once the position and focus have been found, a PSF of angular size large enough to cover the host image is created with these parameters, and it is used in the subsequent analysis.

3.2. Second Step: Distinguishing the QSO and Host Galaxy Light

A second two-dimensional fit distinguishes the light of the QSO from that of the resolved host galaxy, simultaneously fitting both parts. In this step, the model PSF's brightness is scaled to match the QSO nuclear brightness, while a galaxy model is fitted to the host. The host model accounts for ellipticity, position angle, brightness, size, and a simple morphological classification based on radial profile. We consider two surface brightness models, each of which is convolved with the PSF: the de Vaucouleurs $r^{1/4}$ law, $I(\tilde{r}) = I(0) \exp[-7.67(\tilde{r}/\tilde{r}_{1/2})]$, which is typical of elliptical galaxies, and the exponential law, $I(\tilde{r}) = I(0) \exp(-\tilde{r}/\tilde{r}_e)$, typical of spirals. Here, $\tilde{r}$ is the elliptical radius, $\tilde{r} = (x^2 + \alpha^2 y^2)^{1/2}$, where x and y are aligned with the major and minor axes of the ellipse, respectively, and $\alpha = a/b$, where a is the semimajor axis and b is the semiminor axis. The half-light radius $\tilde{r}_{1/2}$ is the elliptical radius enclosing half the total light as projected onto the sky; for the exponential model, $\tilde{r}_{1/2} = 1.68\tilde{r}_e$.

In six cases, namely PG 0052+251, Mrk 1014, PKS 0736+01, 3C 215, LBQS 1222+1010, and PG 1402+261, the automated fitting procedure does not produce a good match to the central point source, most often because of complex host features at very small radii. For these cases, we manually subtract an increasingly luminous central point source until the residuals are smooth. Consequently, the resulting nuclear and host magnitudes for these objects are somewhat subjective and more uncertain.

For ≈90% of the objects, the host morphology is assigned simply on the basis of the best-fitting (lowest χ^2) model: elliptical if the $r^{1/4}$ model fits best, spiral if the exponential model does. We overrule the automatic classification in seven cases. Four hosts, those of PKS 0312−77, PKS 1004+13, PG 1216+069, and PG 1358+04, yield a spiral classification after the automated fit, but plots of their radial profiles (Fig. 1) show them to follow an $r^{1/4}$ law more closely overall [i.e., plotting log (counts) vs. $r^{1/4}$ yields a straight line], and they show no evidence of spiral arms. They are reclassified as ellipticals, and their $r^{1/4}$ models are used in our subsequent analysis. Three hosts, those of Mrk 1014, PG 1309+355, and MS 2159.5−5713, have their radial profiles outside their central bulges well represented by the $r^{1/4}$ law, yet they show clear evidence of spiral arms. They are thus classified as spirals, although their best-fitting $r^{1/4}$ models are used in the analysis. Note that we are able to identify late-type spiral structure in hosts at redshifts as high as $z = 0.4$. Except for these seven cases, we keep the morphological assignments determined by the best-fitting models.

For spiral hosts with a visible bulge, we use masks to fit the bulge and disk separately. The bulge is fitted first, and its model is subtracted from the entire image before the disk is fitted. Bars, if present, are masked out of the fit altogether, although they are used in determining the host's total magnitude. Based on visual inspection, some hosts appear to have undergone recent, strong interactions that have severely distorted their appearances from those of a normal elliptical or spiral, and we have noted these in Table 1. Two QSOs in this sample have a nucleus not concentric with the main part of the host, 3C 48 and IR 0450−2958. Both of these appear to have undergone severe interactions with

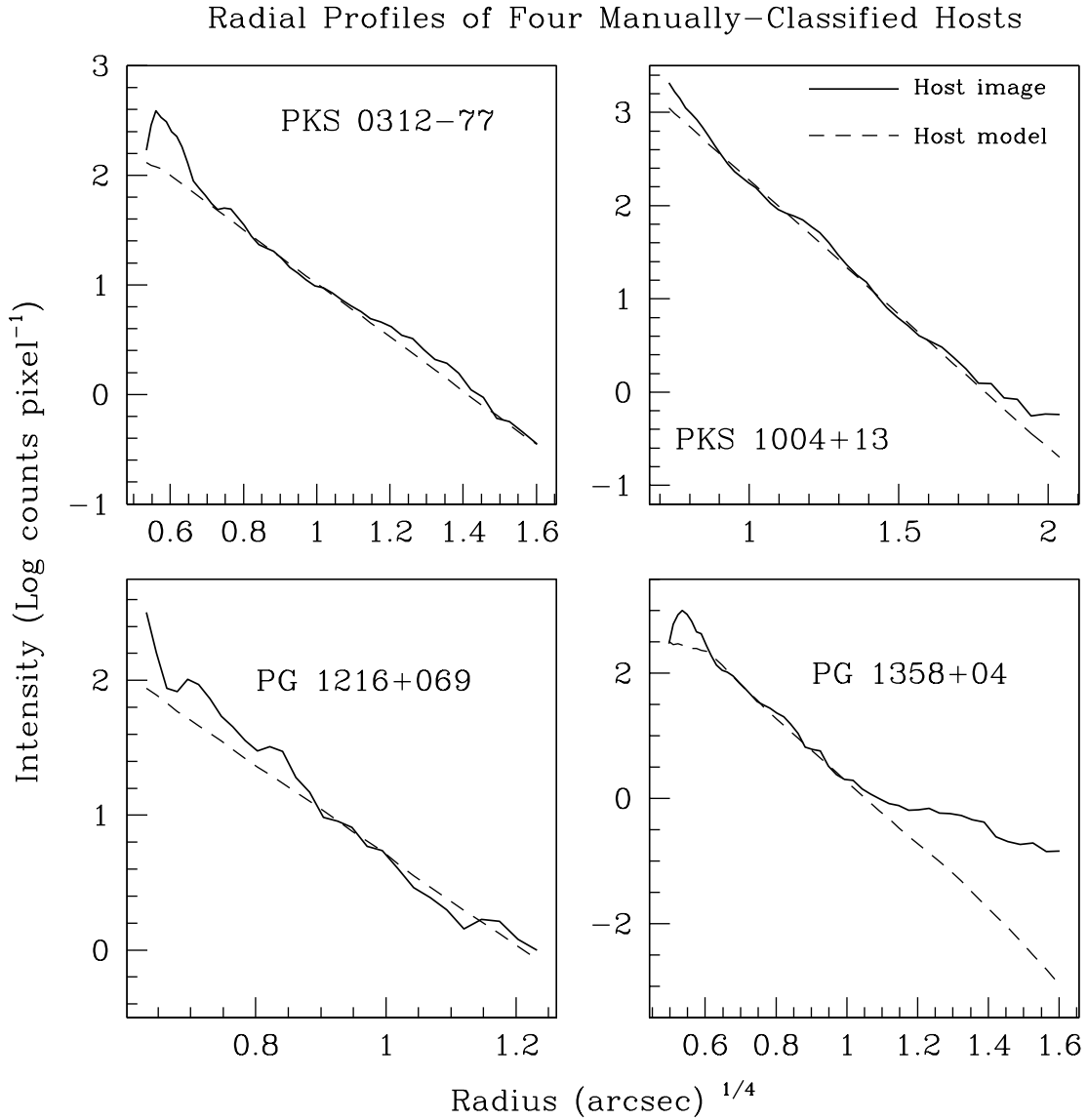## Radial Profiles of Four Manually−Classified Hosts

Fig. 1.—Radial profiles of four manually classified hosts. These are the four, classified as spirals by the automated fit, whose profiles more closely follow an $r^{1/4}$ law, as shown here. The PSFs and sky backgrounds have been subtracted to show the profiles of the underlying hosts (*solid lines*). The profiles of the fitted elliptical host models (*dashed lines*) are shown for comparison. The straightness of the profiles shows that these hosts generally follow the $r^{1/4}$ law. For PG 1358+04, this is true for the bright, inner regions. It has a distinct second component at large radii that is not modeled and is masked from the fit, but this only exists in regions fainter than 1 count pixel^{-1}. The tilt of PG 1216+069's host profile relative to the model is due to the weighting scheme and the imperfect fit of the bright PSF. On the basis of these profiles, all four of these hosts are classified as ellipticals.

other galaxies and are left with disrupted hosts and offset nuclei. There are several other cases of hosts that have undergone interactions, such as Q0316−346, PG 1012+008, and PKS 2349−014, but these still have a nucleus centered within the host.

3.3. *Third Step: Extracting the Magnitudes*

Using the fitted parameters, we then subtract the properly scaled PSF from the QSO image, leaving the host galaxy. The magnitude of the nucleus is measured directly from the scaled PSF model. The light of the PSF model is measured within an aperture of radius 0″.5. An aperture correction of 0.10 mag is subtracted (Voit 1997), and the result is used for the nuclear apparent magnitude. The host magnitude is measured from the PSF-subtracted image, within an aper-

ture large enough to encompass the visible extent of the host. Outside the aperture, we extrapolate the *host model* to a radius of infinity and add this contribution to the light contained within the aperture, yielding the apparent magnitude of the host galaxy. The measurements are not based on the models alone because the host profiles often deviate from strict $r^{1/4}$ or exponential laws, creating noticeable differences between magnitudes derived from the model alone and magnitudes obtained in the way described above. For some objects, we find differences between our host magnitudes and those of other researchers that may be due to their having derived the magnitudes from the host model alone (see §§ 3.4 and 5.4).

With the exception of MRC 0022−297 (which was observed with the F336W filter), the observations were made in WFPC2 F606W or redder filters. The measured

apparent magnitudes of the nuclei and hosts are transformed to rest-frame V. They are then converted to absolute magnitudes in our adopted cosmology and reported in Table 1.

In calculating the absolute V magnitudes, the apparent V magnitudes are first obtained by applying a color correction. Colors for the nuclei are interpolated in redshift from Cristiani & Vio (1990), who provide $V-R$ and $V-I$ as functions of the redshift z (where R corresponds closely to F675W and I to F814W). We obtain colors for $V-$F606W and $V-$F702W by treating these filters as linear combinations of V, R, and I. We calculate the combinations using the IRAF SYNPHOT package and a power-law spectrum of the form $f_\nu \propto \nu^\alpha$, with $\alpha = 0.0$. For the F606W filter, we use $V = $ F606W $+ 0.25(V-R)$, and for the F702W filter, $V = $ F702W $+ 0.85(V-R) + 0.15(V-I)$. For R-band images of redshift $z < 0.1$ and I-band images of redshift $z < 0.2$, Cristiani & Vio (1990) have no color data. We therefore take $V-R = 0.25$ and $V-I = 0.43$, calculated using the above power-law spectrum.

Galaxy colors are interpolated in redshift from Fukugita, Shimasaku, & Ichikawa (1995). Because we do not classify the spiral galaxies into more detailed morphologies, we average together the colors given for the S0 and all spiral categories in Fukugita et al. (1995). There are noticeable differences in the $V-$F814W colors of S0 and Scd galaxies at higher redshifts. At a redshift of $z = 0.0$, the maximum deviation from the average is ≈ 0.05 mag, but this grows to 0.26 mag at a redshift of $z = 0.5$. The other spiral colors have much smaller differences.

Once we have the apparent V magnitudes, the absolute V magnitudes are given by

$$M_V = m_V - 45.396 - 5\log\left(1 + z - \sqrt{1+z}\right)$$
$$- K(V) - A_V , \qquad (1)$$

where $K(V)$ is the V-band K-correction, and A_V is the Galactic reddening. The individual absolute magnitudes here account for Galactic extinction, using the data from Schlegel, Finkbeiner, & Davis (1998) and interpolated by the Galactic extinction calculator on NED.[5] The unweighted and weighted host luminosity distributions use the extinction-corrected magnitudes, but the host luminosity function uses the uncorrected magnitudes. This is done to allow a direct comparison with the luminosity function of Metcalfe et al. (1998), which does not account for Galactic extinction. We interpolate the nuclear K-corrections in redshift from the data of Cristiani & Vio (1990). For galaxy K-corrections, we use the data of Pence (1976), who assumes no intrinsic reddening in the host galaxies. Pence (1976) combines elliptical and S0 morphologies into a single category and subdivides spiral galaxies into multiple categories. Following our decision with spiral galaxy colors, we average the K-corrections for all spiral types, including S0. At a redshift of $z = 0.06$, the maximum deviation from this average is 0.06 mag, and at a redshift of $z = 0.46$, this increases to 0.49 mag.

3.4. Comparison with Other Methods

The analysis techniques used by others in studies with criteria similar to our own are sometimes different in minor

ways. For example, the method of Bahcall et al. (1997) uses stellar PSFs taken at the time of the observations, while we generally cannot. They observe a set of four stars for the PSFs, chosen to have colors similar to those of QSOs. The PSF is subtracted by scaling it until the χ^2 between it and the QSO image is minimized. The best-fitting of the four PSF stars is used in each case. Elliptical and spiral host models are then fitted to the residual in an annular region $r > 1\farcs0$, avoiding the core of the QSO. Bahcall et al. (1997) try one- and two-dimensional models and adopt the two-dimensional results in the end.

McLure et al. (1999) also use stellar observations for the PSFs in their analysis, employing two-point dithering to improve the sampling (and therefore the subpixel centering), with the PSF stars being chosen to match closely the typical $B-V$ colors of QSOs. Their host-fitting technique is similar to ours, with the host and QSO being fitted simultaneously. They use a two-dimensional host model, assuming either a strict $r^{1/4}$ or exponential law profile and varying the host model's size, luminosity, ellipticity, and position angle, as well as the nuclear luminosity. Separately, they try the technique of using a model with the radial profile having a variable exponent β. A true exponential law would have $\beta = 1.00$, and a de Vaucouleurs law would appear as $\beta = 0.25$. They achieve similar classifications using this technique, but their adopted M_{host}-values are based on the former method.

4. THE LUMINOSITY FUNCTION OF QSO HOST GALAXIES

4.1. Subclasses and the Unweighted Absolute Magnitude Distribution of QSO Hosts

With 70 detected QSO hosts in our sample, we are able to investigate the properties of the host galaxy luminosity function quantitatively and to consider issues related to host morphology and radio loudness.

As noted in § 2, the host of one QSO is not convincingly detected; this one, MRC 0022$-$197, is a radio-loud QSO and is the only QSO observed in the F336W filter (approximately Johnson U). Importantly, this is also the QSO in our sample with the faintest apparent magnitude, $m_V = 19.0$, according to Véron-Cetty & Véron (1998). For one spiral (MS 2159.5$-$5713), we have no radio information. Consequently, MRC 0022$-$197 is excluded from all analyses, and MS 2159.5$-$5713 is excluded from analyses requiring radio information.

It is of interest to consider whether the remaining elliptical and spiral hosts in our sample are drawn from different parent populations. This might also be related to possible selection effects and biases (§ 5.3). Below, we consider these objects in terms of a binary classification yielding four subclasses. The nuclear and host magnitudes for these objects, separated by subclass, are plotted in Figure 2. The overall absolute magnitude distribution of the hosts in our sample is shown in Figure 2. Our sample is divided almost evenly into three subclasses: radio-loud QSOs with elliptical hosts (designated "LE," 22 objects), radio-quiet QSO with elliptical hosts (designated "QE," 22 objects), and radio-quiet QSOs with spiral hosts (designated "QS," 21 objects). Membership in the fourth subclass, radio-loud QSOs with spiral hosts (designated "LS," four objects), is rare. The total of these subsamples is 69 because the lack of radio
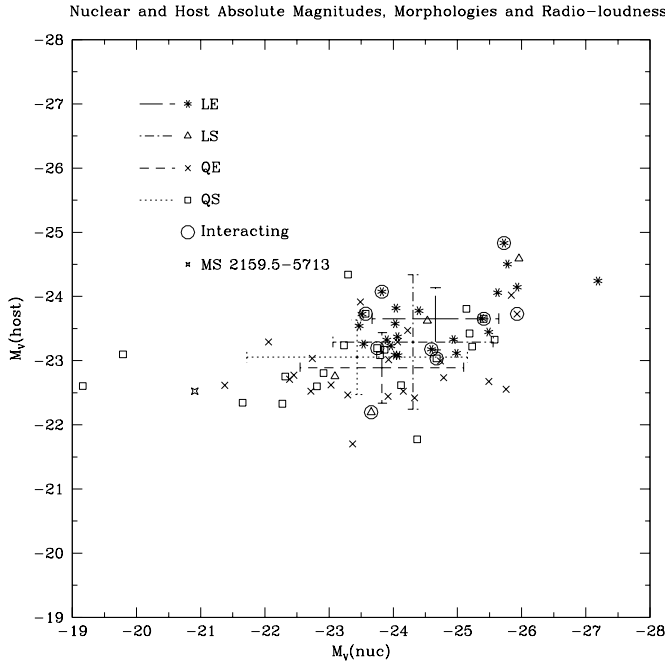
FIG. 2.—Distribution of morphological and radio properties of the sample with respect to host and nuclear luminosities. "LE" refers to radio-loud QSOs in ellipticals, "QE" to radio-quiet QSOs in ellipticals, "QS" to radio-quiet QSOs in spirals, and "LS" to radio-loud QSOs in spirals. The rms error bars for each subclass are overlaid, centered on the mean of each distribution according to the legend.

information on MS 2159.5−5713 excludes it. First we discuss the rare LS subclass.

Two of the four radio-loud QSOs with spiral hosts, 3C 277.1 and MC 1548+114A, are at redshifts $z > 0.3$ and have little detail visible, but both appear to have large tidal arms that may be responsible for the exponential profile's being the better model. It is possible that they are simply interacting cases and not normal spirals. In addition, 3C 277.1 is a compact, steep-spectrum quasar known to have bright, emission-line gas aligned with the radio source, and its classification may have been affected by this feature (de Vries et al. 1999). A third object, 3C 351, appears to contain a complete ring surrounding an off-center bulge, with the putative bulge following an $r^{1/4}$ radial profile. We classify the complete host as a spiral on the basis of the ring structure, although it could be another case of an interacting system. The fourth, PG 1309+355 ($z = 0.184$), has spiral arms but follows an $r^{1/4}$ profile. Its unitless radio-to-optical flux density ratio is ≈ 18 (Kellermann et al. 1989). Since Kellermann et al. (1989) classify QSOs with radio-to-optical flux ratios greater than 10 as radio-loud, it would be considered radio-loud by that standard. However, its ratio does lie between the peaks of the radio-loud and radio-quiet distributions. Furthermore, its observed 6 cm flux is only ≈ 54 mJy, despite its low redshift. Therefore, it, too, might be considered a questionable case for a radio-loud spiral.

Thus, with the possible exceptions of PG 1309+355 and 3C 351, we confirm the result of Bahcall et al. (1997) that radio-loud QSOs are almost exclusively found in elliptical or interacting hosts, while radio-quiet QSOs may be found in elliptical, spiral, or interacting systems. The host absolute magnitudes of the radio-loud spirals were found to lie in the

range $-22.2 > M_V > -24.6$, spread across our overall host absolute magnitude distribution.

Table 2 presents the median absolute magnitudes of the various subsamples. To check whether the host and nuclear luminosities in each of the three major subclasses are consistent with being drawn from similar parent populations, we apply two-sample Kolmogorov-Smirnov (K-S) tests to each combination of subclasses. The detailed results of this exercise are reported in Table 3. The individual host magnitude distributions are shown in Figure 3. Comparison of the LE and QE subclasses shows that their host luminosity distributions differ at a significance greater than 99.9%, while their nuclear luminosity distributions differ at a significance of 96.5%. Formally, the LE subclass is more luminous than the QE subclass in both cases. For host magnitudes, the LE median is 0.8 mag brighter than the QE median, but for nuclear magnitudes the LE median is only about 0.2 mag brighter than that of the QE class. Comparison of the LE and QS subclasses shows that both their host and nuclear luminosity distributions differ at a significance greater than 97%, with the LE subclass again being the more luminous. The LE median host magnitude is about 0.4 mag brighter than the QS median, and the LE median nuclear magnitude is about 0.3 mag brighter than that of the QS class. The host luminosity distributions of the QE and QS subclasses are slightly less distinct, differing at a significance of 88.1%, but their nuclear luminosity distributions are fairly compatible, differing only at a significance of 9.2%.

TABLE 2
MEDIAN ABSOLUTE MAGNITUDES OF SUBCLASSES

Subclasses[a]	Members	Median M_V(host)	Median M_V(nuc)
All................	70	−23.18	−24.03
LE................	22	−23.54	−24.08
QE	22	−22.71	−23.92
LS	4	−22.76	−23.66
QS................	21	−23.10	−23.75
L	26	−23.54	−24.08
Q..................	43	−23.00	−23.80
E	44	−23.26	−24.07
S	26	−23.08	−23.30

[a] LE, radio-loud QSOs in elliptical hosts; QE, radio-quiet QSOs in elliptical hosts; QS, radio-quiet QSOs in spiral hosts; L, radio-loud QSOs; Q, radio-quiet QSOs; E, elliptical hosts; S, spiral hosts.

TABLE 3
KOLMOGOROV-SMIRNOV TEST RESULTS FOR SUBCLASS COMPARISON

Subclasses (members)[a]	D_{host}	p_{host}	D_{nuc}	p_{nuc}
LE (22), QE (22)........	0.682	2.75×10^{-5}	0.409	0.0356
LE (22), QS (21)	0.487	7.50×10^{-3}	0.437	0.0222
QE (22), QS (21)........	0.346	1.19×10^{-1}	0.165	0.908
L (26), Q (43).............	0.504	2.83×10^{-4}	0.380	0.0131
E (44), S (26)	0.215	3.91×10^{-1}	0.297	0.0900

NOTES.—The parameter D is the K-S statistic. The parameter p is the probability of obtaining D if the objects in both subclasses are drawn from the same parent population.

[a] LE, radio-loud QSOs in elliptical hosts; QE, radio-quiet QSOs in elliptical hosts; QS, radio-quiet QSOs in spiral hosts; L, radio-loud QSOs; Q, radio-quiet QSOs; E, elliptical hosts; S, spiral hosts.
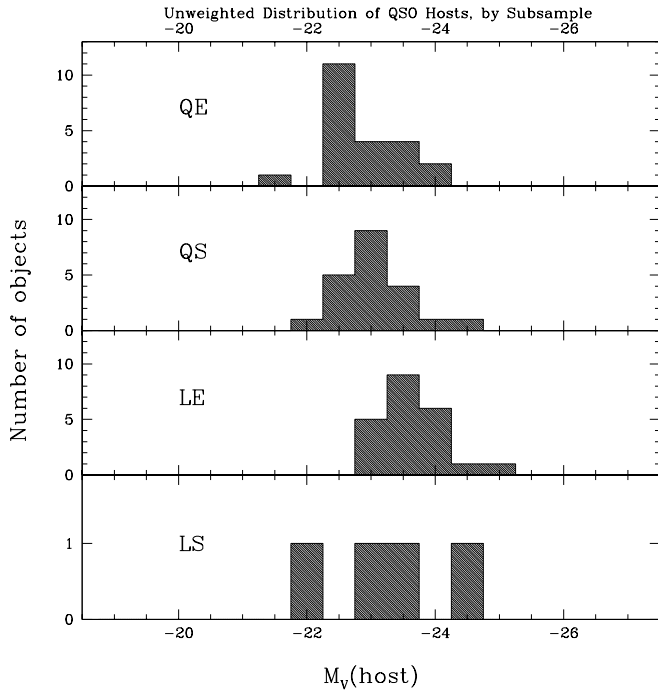
FIG. 3.—Individual host distributions of radio-quiet QSOs in ellipticals (QE), radio-quiet QSOs in spirals (QS), radio-loud QSOs in ellipticals (LE), and radio-loud QSOs in spirals (LS). Note that the vertical axes cover the same range for all but the LS subsample.

FIG. 4.—Unweighted absolute magnitude distribution function of all QSO hosts. The narrow width of the distribution is evident.

In addition, we compare the host and nuclear luminosities of all ellipticals ("E," 44 objects) with those of all spirals ("S," 26 objects), and the host and nuclear luminosities of all radio-loud QSOs ("L," 26 objects) with those of all radio-quiet QSOs ("Q," 43 objects). The results are also shown in Table 3 and indicate that the radio-loud and radio-quiet objects can be distinguished not only by their nuclear luminosity distributions (98.7% significance) but by their host luminosity distributions as well (greater than 99.9% significance). The hosts of radio-loud QSOs are typically half a magnitude more luminous than their radio-quiet counterparts, and the radio-loud nuclei are also noticeably brighter (0.3 mag) than the radio-quiet nuclei. The differences between objects in ellipticals and spirals are less significant, however. Their nuclear luminosity distributions are distinguishable, differing at a significance of 91.0%, but their host luminosity distributions differ only at a 60.9% level of significance. The ellipticals are more luminous than the spirals in both cases. The magnitude difference is fairly small ($\approx$0.2 mag) in their median host magnitudes, but it is pronounced ($\approx$0.8 mag) in their nuclear magnitudes.

From Figure 4 we see that the number distribution of our complete sample of QSO hosts as a function of their absolute magnitude. This distribution is entirely contained within a range of 3.1 mag, from $M_V = -21.7$ to -24.8, with a median of $M_V = -23.2$. It can be fitted by a Gaussian with a peak at $M_V = -23.1$ and a 1 σ width of 0.67 mag. Note that since all but one of the hosts are clearly detected, the lack of faint hosts is not due to a failure to detect them.

4.2. The Weighted Number Distribution of QSO Host Absolute Magnitudes

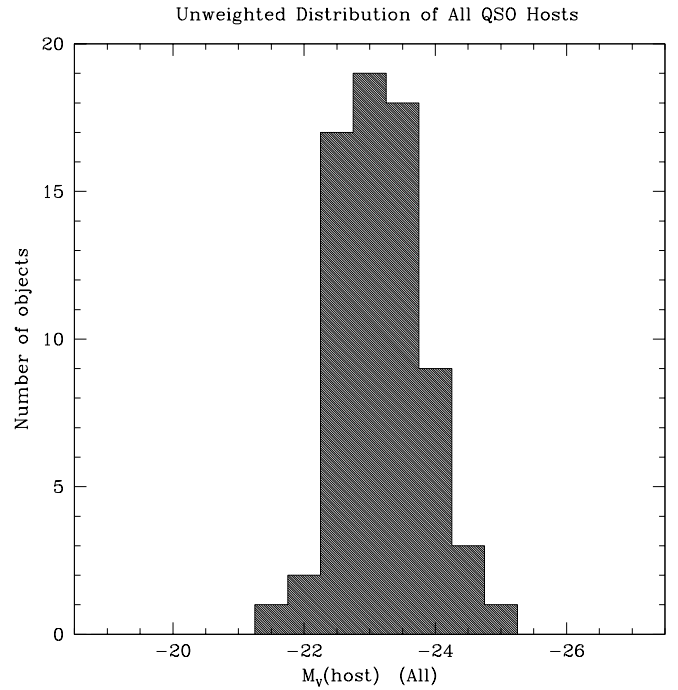The 71 QSOs in our sample correspond to $\approx$7% of all known QSOs within the magnitude range of our sample in

the catalog of Véron-Cetty & Véron (1998; hereafter VCV). However, since our selection of QSOs to include in this study is based on the availability of *HST* observations, they may not adequately represent the characteristics of all low-redshift QSOs. In particular, our sample may be systematically biased as a function of apparent luminosity and redshift: nearer and brighter objects are more accessible and therefore more likely to be selected for study. We therefore apply a simple weighting technique to approximately correct for redshift- and magnitude-dependent selection effects relative to the VCV catalog. However, we note that any inherent biases in the VCV catalog will not be removed. This catalog is intended to be a compilation of all known, published QSOs, so it has a mix of biases from the various surveys that make up the catalog. As a result, for example, its ratio of the number of radio-loud to the number of radio-quiet QSOs is not the true ratio, but we do not base our conclusions on this information. More subtle biases, such as those involving limiting magnitudes, will remain.

Our procedure for weighting the distribution function to derive a corrected or unbiased distribution function is based on a replacement method as follows. For each of the 982 QSOs in VCV within our selected magnitude and redshift range, we pick a representative object in our observed sample with approximately the same total (nuclear plus host) magnitude M_{tot} and redshift z. The representative object is chosen randomly, with a Gaussian probability distribution that depends on the difference in absolute magnitude and redshift. We choose a Gaussian width of 0.5 mag in absolute magnitude and 0.07 in redshift. These widths are chosen to ensure that most catalog objects have several sample objects within about 1 σ in both magnitude and redshift; if the widths are too narrow, regions of the (M_{tot}, z) plane that contain few sample objects would yield a luminosity function that depends too heavily on those few objects.

Each object, i, in our observed sample is then assigned a weight, w_i, that is simply the number of times it is selected by the random process. The resulting weighted distribution function is shown as the unshaded histogram in Figure 5. The error bars reflect the nominal counting error defined as $\sigma_{\mathrm{bin}} = \left[\Sigma_i\left(w_i^2\right)\right]^{1/2}$, where the sum is over all objects in the bin. Note that this error is an upper limit for the Poisson uncertainty in the distribution function in that bin, in that it assumes that the host magnitude is not correlated with redshift or total magnitude; any correlation makes the assignment process less random and therefore reduces the counting uncertainty.

The extinction-corrected, weighted distribution function has a shape similar to that of the unweighted distribution, although with a narrower peak, and its estimated median, $M_V \approx -23.23$, is almost identical. A Gaussian fit to the weighted distribution peaks at $M_V = -23.1$ and has a $1\,\sigma$ width of 0.63, so it peaks approximately in the same location as the fit to the unweighted data and has only a slightly narrower width.

Since the morphologies of VCV hosts are generally unknown, we cannot weight the elliptical and spiral distributions separately. However, we can perform a simple weighting for radio loudness by using the unitless radio-to-optical flux density ratio, R_{ro}, described by Kellermann et al. (1989), calculated from the apparent V magnitudes and the 6 cm radio flux densities listed in VCV. Since these are relatively nearby QSOs, we assume those QSOs without radio detections in VCV to have no 6 cm flux. Kellermann et al. (1989) classify QSOs with $R_{\mathrm{ro}} > 10$ as radio-loud and those with $R_{\mathrm{ro}} < 1$ as radio-quiet. In keeping with Brinkmann et al. (1997) and Yuan et al. (1998), we choose $R_{\mathrm{ro}} = 10$ as a strict dividing line between radio-loud and radio-quiet. Under these assumptions, we derive a weighted distribution function of QSO hosts, separated in terms of hosts of radio-loud and radio-quiet QSOs. These individual weighted distributions are also shown in Figure 5. The shapes of the radio-loud and radio-quiet distributions are fairly similar between the weighted and unweighted versions. Note that the weighted radio-quiet distribution rises higher than the overall weighted distribution in some bins. This is because they are calculated from separate Monte Carlo runs.

4.3. The Luminosity Function of QSO Host Galaxies

We use the QSO luminosity function of Boyle et al. (2000) to derive a normalization for our weighted host distribution function, turning it into a QSO host galaxy luminosity function. Boyle et al. (2000) have analyzed a ground-based sample of over 6000 QSOs to derive a QSO luminosity function for the total (nuclear plus host) light. They parameterize the luminosity function in terms of a two–power-law function,

$$\Phi(M_B, z) = \Phi^*_{\mathrm{Boyle}}\left\{ 10^{-0.4\left(\alpha_{\mathrm{Boyle}}+1\right)\left[M_B - M_B^*(z)\right]} \right.$$
$$\left. + 10^{-0.4\left(\beta_{\mathrm{Boyle}}+1\right)\left[M_B - M_B^*(z)\right]} \right\}^{-1}, \quad (2)$$

and use a polynomial function for the evolution of $M_B^*(z)$ in redshift, $M_B^*(z) = M_B^*(0) - 2.5(k_1 z + k_2 z^2)$, where $\alpha_{\mathrm{Boyle}} = 3.60$, $\beta_{\mathrm{Boyle}} = 1.77$, $M_B^*(0) = -22.39$, $k_1 = 1.31$, $k_2 = -0.25$, and $\Phi^*_{\mathrm{Boyle}} = 6.8 \times 10^{-7}$ objects Mpc^{-3} mag^{-1}. Their data are limited to redshifts of $z \geq 0.35$, and at the low-redshift end the data do not span a large range in total absolute magnitude. Thus, we restrict our consideration to redshifts of $0.35 \leq z \leq 0.46$, where our sample overlaps with theirs, and to total absolute magnitudes of $-23.00 \geq M_V(\mathrm{total}) \geq -24.61$, extending no more than 1 mag brighter than $M_B^*(z = 0.405)$. We use $z = 0.405$ in the function, since it is the average of the range we consider. We note parenthetically that 22 of the QSOs in our sample lie within this redshift range and that 12 of those also lie within the above total magnitude range. Since the total absolute magnitudes of the QSOs in the survey of Boyle et al. (2000) are likely dominated by nuclear luminosity, we assume $B - V \approx 0.0$.

Integrating the two–power-law function over the range $-23.0 \geq M_V(\mathrm{total}) \geq -24.61$, with $z = 0.405$, we find 7.5×10^{-7} QSOs Mpc^{-3}. Over the same total absolute magnitude interval, with $0.35 \leq z \leq 0.46$, there are 228 objects in the VCV catalog. Dividing the integrated function by 228, we obtain a normalization factor of 3.3×10^{-9} Mpc^{-3}. Multiplying our weighted host distribution by this normalization factor, and by a factor of 2 to account for our 0.5 mag bin width, converts our distribution into a QSO host luminosity function in units of QSO hosts Mpc^{-3} mag^{-1}. This QSO host luminosity function is shown in Figure 6. We note that in Figure 6 we also show how removing objects with nuclear luminosities fainter than $M_V = -23$ affects the derived luminosity function.
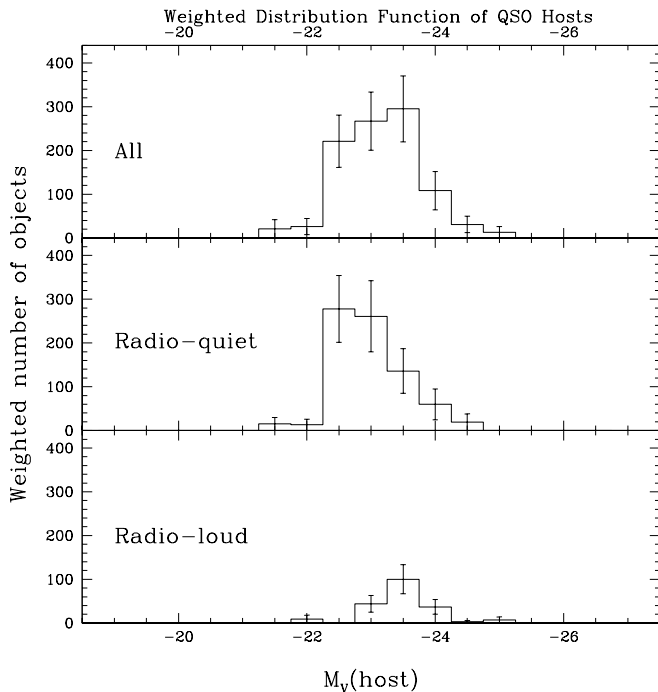

Fig. 5.—Weighted absolute magnitude distribution functions of QSO hosts. The distribution for the complete sample is shown, as well as the distributions for the radio-quiet and radio-loud subsamples. Note that the radio-quiet distribution has a higher population than the total distribution in some bins, because they are calculated from separate Monte Carlo runs.

5. DISCUSSION

Here we elaborate on some of the results of this work. A more thorough discussion will be made elsewhere when we consider the other properties of the sample in detail.

QSO Host and Normal Galaxy Luminosity Functions

Normal Galaxy LF
— — Normal Galaxy LF
(Extrapolated)
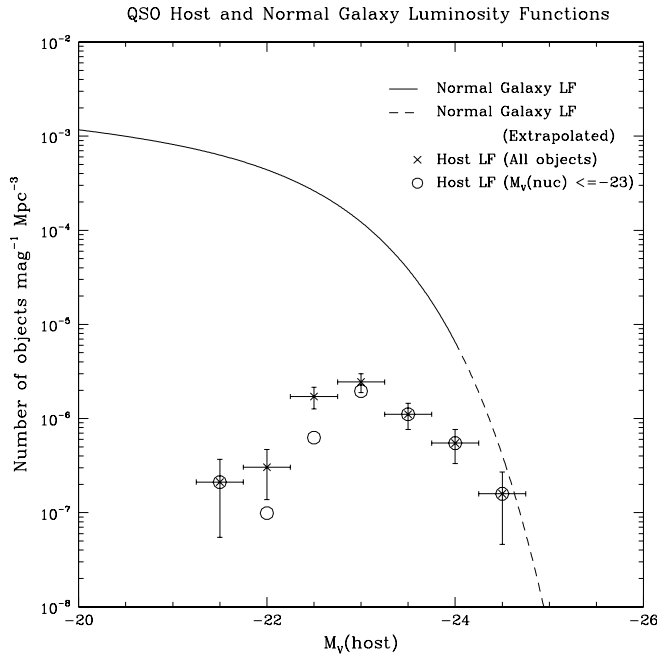× Host LF (All objects)
○ Host LF (M_V(nuc) <=−23)

FIG. 6.—Combined luminosity function of QSO host galaxies for our sample, compared with the normal galaxy luminosity function of Metcalfe et al. (1998). The dashed line shows the extrapolated region of the normal galaxy luminosity function. Crosses show the derived luminosity function for the entire sample, while circles show the derived luminosity function for QSOs with nuclear magnitudes brighter than $M_V = -23$.

5.1. Comparison of the QSO Host and Normal Galaxy Luminosity Functions

To compare our QSO host galaxy luminosity function (§ 4.3) with that of normal galaxies, we use the normal galaxy luminosity function of Metcalfe et al. (1998). The Schechter (1976) luminosity function parameters that describe their V-band luminosity function in our cosmology are $\alpha = -1.2$, $M_V^* = -22.35$, and $\Phi^* = 8.5 \times 10^{-4}$ Mpc^{-3}. The host luminosity function lies below that of normal galaxies, as shown in Figure 6. The most relevant uncertainty in the normal galaxy luminosity function is at the bright end, where it is less well constrained because of the dearth of luminous galaxies in surveys. The least luminous QSO host used in our analysis is relatively luminous, with $M_V = -21.7$, and the median of our QSO host luminosity function is at $M_V \approx -22.95$, twice the luminosity of the M_V^* "knee" of the normal galaxy luminosity function. The normal galaxy luminosity function is also shown in Figure 6, and it is evident that it has a shape very different from that of the QSO luminosity function.

The brightest luminosity bin in the Metcalfe et al. (1998) data extends up to $M_V \gtrsim -24.0$, and their Schechter function is extrapolated to brighter magnitudes, as we have marked with the dashed line in Figure 6. In fact, we searched for published accounts of any normal galaxies of luminosity $M_V < -24.0$, with little success. The Sloan Digital Sky Survey has recently released a preliminary galaxy luminosity function (Blanton et al. 2001), in which the highest-luminosity bin also extends up to $M_V \gtrsim -24.0$. We also searched the literature on brightest cluster galaxies (BCGs). In the sample of BCGs in Postman & Lauer (1995), the most luminous has $M_V \approx -23.7$, although Disney et al. (1995) refer in passing to BCG luminosities as $M_V \approx -24.5$. It may be that

the $M_V < -24.0$ region is dominated by QSO hosts. We conclude that the luminosity function of QSO hosts differs greatly in shape from that of normal galaxies but that they are coincident in the highest-luminosity bin, if the normal galaxy luminosity function can be extrapolated that far.

We can use the luminosity functions to estimate the ratio of the number of low-redshift QSO hosts to the number of normal galaxies as a function of absolute magnitude. The normal galaxy luminosity function is integrated over our 0.5 mag bins and then compared with the binned host data. The ratio of the number of hosts to the number of normal galaxies is shown in Figure 7, along with a parameterization of the results. The relationship can be expressed as $\mathscr{R} = \left(L_V/11.48 L_V^*\right)^{2.46}$, up to $M_V \approx -25.0$, where $\mathscr{R}$ is the ratio of the number of hosts to the number of normal galaxies, L_V is the V-band luminosity, and L_V^* corresponds to $M_V^* = -22.35$. The points at $M_V = -24.0$ and -24.5 are drawn with thin lines to indicate that they depend on the extrapolation of the normal galaxy luminosity function, although they are included in the fit. We note that the accuracy of these results is subject to the inherent systematic uncertainties in normalization procedures for both the local galaxy luminosity function and our low-redshift QSO host galaxy luminosity function. Normalizations of normal galaxy luminosity functions can differ by a factor of 2 from one study to another.

The conclusions drawn here about the comparison of the QSO and normal galaxy luminosity functions are roughly similar to those reached by Smith et al. (1986) in their ground-based study of the hosts of QSOs and lower luminosity active galactic nuclei. The current data are of course

Ratio of QSO Hosts to Normal Galaxies

—— Fitted relation using all objects
— — Fitted relation using M_V(nuc) <= −23
× Ratio using all objects
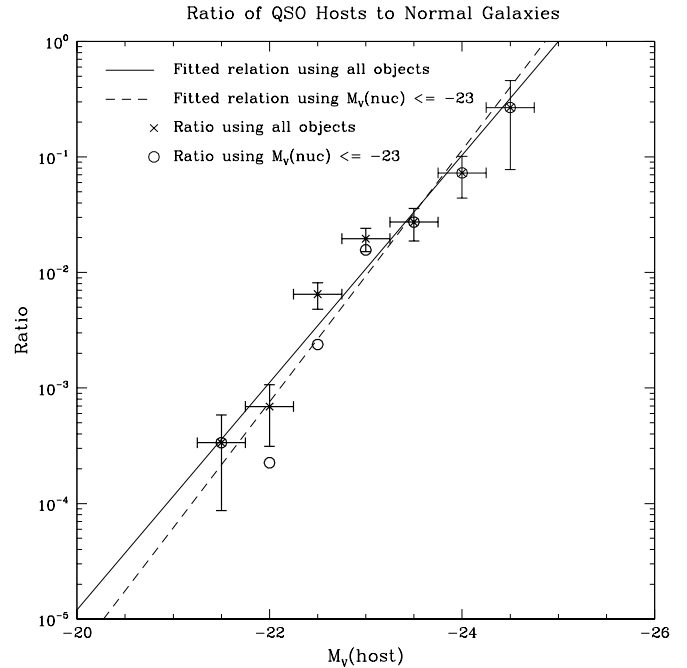○ Ratio using M_V(nuc) <= −23

FIG. 7.—Low-redshift QSO host galaxy luminosity function divided by the normal local galaxy luminosity function, yielding the probability that a galaxy of absolute magnitude M_V will host a QSO. Crosses show this result for the entire sample, while circles show this result for QSOs with nuclear magnitudes brighter than $M_V = -23$. The solid line shows the fit specified in the text for all hosts, while the dashed line shows the fit for QSOs with M_V(nuc) ≤ -23. The upper two points, drawn with thin lines, are in the extrapolated region of the normal galaxy luminosity function.

better than what was available to them, so we believe that the conclusions are now considerably stronger. As suggested by these authors, this ratio essentially represents an empirical parameterization of the probability that a galaxy with luminosity L_V will host a QSO. It applies in the redshift interval studied here, $z \approx 0.06$–0.46.

5.2. Radio-loud and Radio-quiet QSOs with Elliptical Hosts

As described in § 4.1 and shown in Figures 2 and 3, the QE subclass tends to have dimmer host and nuclear luminosities than the LE subclass, but there is a great deal of overlap. Within this overlap, there must be some property, other than host luminosity, that affects the amount or nature of the fuel available to the central engine for radio emission. The possible causes of this effect should be investigated more closely by using the members of these two subclasses of elliptical hosts to examine other properties of these QSOs, including environmental clues.

5.3. Selection Effects and Biases

Images in our sample are of heterogeneous quality, because the original observers have chosen a variety of filters and exposure times for objects with disparate properties. The best-exposed images, such as Q1402+436 and PG 1444+407, average up to 15,000 e pixel^{-1} within the half-light radius, for a signal-to-noise ratio (S/N) up to 150 per resolution element (the FWHM of the PSF). The worst cases, such as 3C 93 and LBQS 0020+0018, have as little as 200 e pixel^{-1}, for an S/N of 25 per resolution element. Adequate model fits can be obtained even in images with low S/N, as shown by the radial profile of 3C 93 (Fig. 8).
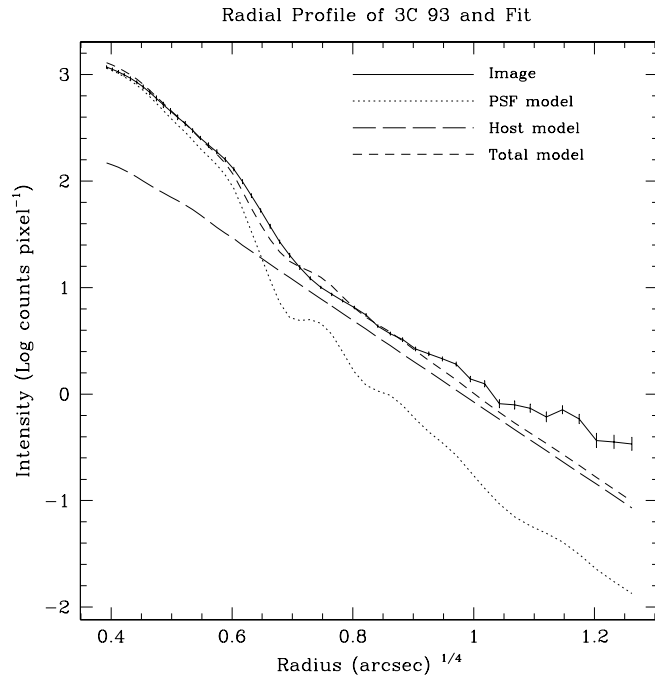
While noise does give its profile a ragged appearance, the model is not a bad fit overall, and the small discrepancy between model fit and measured profile is not reflected in the object's computed magnitude, which is based primarily on the actual counts rather than on the model fit (§ 3.3). Some of the most irregularly shaped hosts can give rise to systematic differences between the image profile and the model, as in the example of 3C 48 (Fig. 9). In this case, the host's shape and position, with the active nucleus offset from its center, requires masking irregular parts of the host to allow the fit to converge; this results in the systematic errors at small radii shown in the figure. But others of these irregular hosts, such as PKS 2349−014 (Fig. 10), have excellent fits, without significant systematic differences in their profiles. Finally, Figure 11 shows an example of a spiral host with both the disk and bulge modeled.

A bright QSO may be expected to hide a dim host, and the more distant it is, the harder the host will be to detect. However, we are able to see hosts that are 3.3 mag dimmer than their nuclear QSO light (in apparent magnitudes in the observed wave bands). Very few of the objects have hosts nearly this much dimmer than their nuclei, and there are in fact only seven objects that have a host 2.1 or more mag dimmer than their nucleus. In general, considering that the host magnitudes span a noticeably smaller range than the nuclear magnitudes (Fig. 2), combined with the fact that we have failed to detect a host in only one case, makes us confident that our host luminosity function is not strongly biased by missing very dim hosts.

The ellipticals outnumber the spirals in our sample, making up 62% of the total. However, because of *HST* target selection effects, this may not be representative of all QSOs

Fig. 8.—Radial profiles of 3C 93 (*solid line*) and model. Error bars on the image profile represent uncertainties in the elliptical isophotes used to plot the profile. The model PSF is represented by the dotted line, the model host by the long-dashed line, and the total model by the short-dashed line. Because of the low S/N, the model is not a perfect match to the image profile. Note the deviation of the host from a strict $r^{1/4}$ law profile at large radii. Although this feature is not fitted by the model, the extra light is included in the host magnitude.
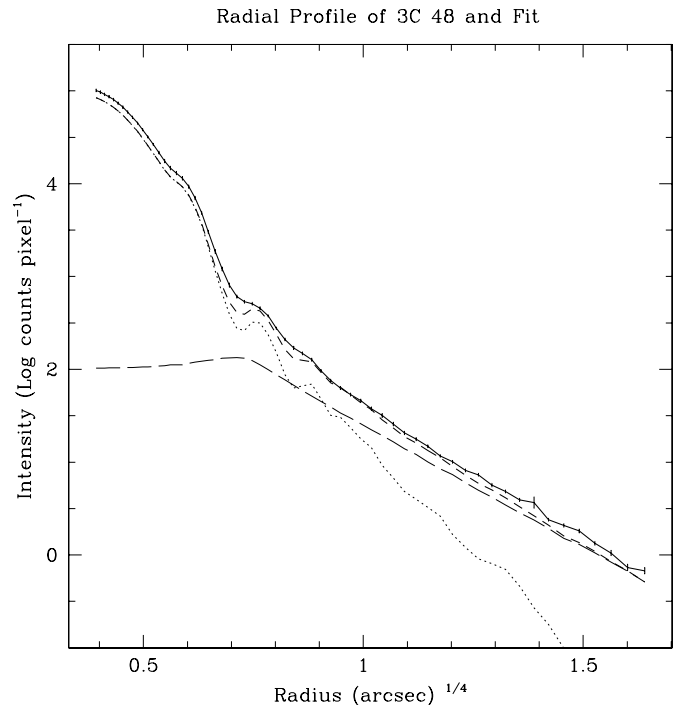

Fig. 9.—Same as Fig. 8, but for 3C 48. The higher S/N makes a smoother profile than in the case of 3C 93, but the irregular host shape causes the model to underestimate the light at small radii slightly. The turnover of the host profile is due to its center being offset from the QSO nucleus by 0″.25.
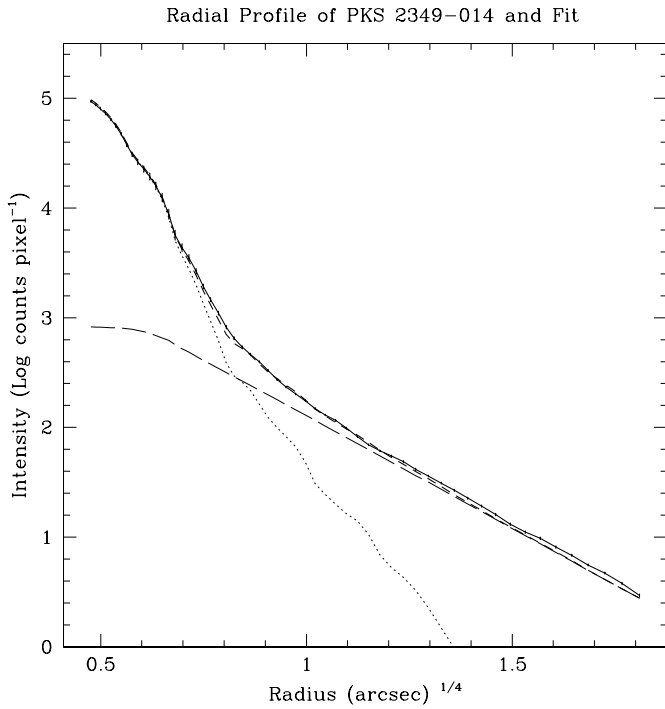
Radial Profile of PKS 2349−014 and Fit

FIG. 10.—Same as Fig. 8, but for PKS 2349−014. Despite the irregularity of the host morphology, a good fit to the profile is obtained.
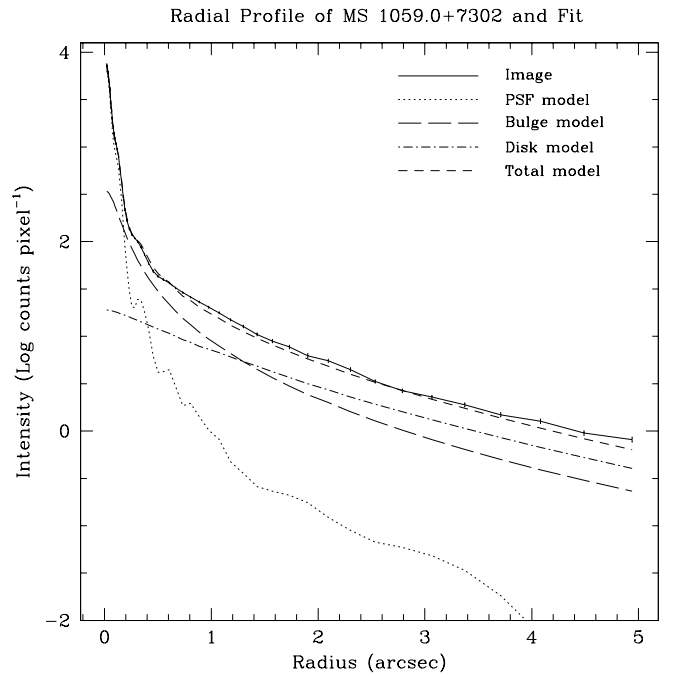
Radial Profile of MS 1059.0+7302 and Fit

FIG. 11.—Radial profiles of MS 1059.0+7302 (*solid line*) and model. Note that line styles and axes differ from the previous figures. The dotted line represents the PSF model, the long-dashed line the bulge model, the dot-dashed line the disk model, and the short-dashed line the total model. This QSO has a spiral host with a bulge and a disk. The profile is not perfectly smooth but is fairly well modeled. The host model is slightly fainter than the image profile at large radii, but the excess light is included in the host magnitude.

in this redshift range. For example, we confirm, with only one or two possible exceptions, that radio-loud QSOs are found in elliptical or interacting hosts (§ 4.1), while radio-quiet QSOs may be found in either ellipticals, spirals, or interacting cases. The fraction of radio-loud QSOs in our sample is ≈37%, higher than the 10%–20% expected for optically selected samples in this redshift range (Kellermann et al. 1989; Hooper et al. 1995, 1996). This may indicate that we have selected an artificially high fraction of QSOs with elliptical hosts. But since QSOs in ellipticals are more luminous than those in spirals, our weighting procedure (§ 4.2) may compensate for this bias to an extent.

It is unlikely that a redshift-dependent magnitude bias could arise from nonstellar emission from the hosts. Spiral hosts may contain H II regions; however, most bright H II regions are masked from our fits and analyses if they are in dim areas of the host. Although less prominent H II regions might be unmasked, the rest equivalent width of Hα, the major H II emission line, is typically ∼25 Å in late-type galaxies (Gavazzi et al. 1998). In contrast, the WFPC2 wideband filters we use have much larger equivalent widths, ranging from 867 Å (F675W) to 1539 Å (F814W) (Biretta et al. 1995), so the Hα effect in the host is very small. More important is the effect that broad emission lines might have on a QSO's nuclear luminosity, and Hα is again the most prominent line. In this case, Hα rest-frame equivalent widths are distributed with a median of ≈240 Å and usually do not exceed ≈450 Å (Sabbey 1999);[6] thus, this could account for at most a few tenths of a magnitude variation, depending on whether or not the line is included in the filter passband.

5.4. *Comparisons with Results from Some Other Studies*

There have been a few other large-sample studies of QSO hosts with selection criteria similar to our own. Of the space-based *HST* ones, the two largest, those of Bahcall et al. (1997) and of McLure et al. (1999), have samples that are included in ours.

The sample of Bahcall et al. (1997) includes 20 QSOs with redshifts $z < 0.3$ and $M_V < -24.4$, making them among the most luminous objects in the nearby universe. In this comparison, we use their final results, which come from their two-dimensional model fits. Their host magnitude distribution has a shape similar to ours but is nearly 1 mag fainter. It should be noted that the results of their one-dimensional fits are brighter than those of their two-dimensional fits and give a distribution about half a magnitude fainter than ours. They find that, on average, the hosts of radio-loud QSOs are 1 mag brighter than the hosts of radio-quiet QSOs, while we find that the radio-loud hosts are about half a magnitude brighter. They also report the hint of a luminosity difference between elliptical and spiral hosts, but they state that it may be artificial, a consequence of fitting the host model to the outer ($r \geq 1{\farcs}0$) region of the host. Our analysis shows only a small difference, with elliptical hosts being ≈0.2 mag brighter than the spirals on average. This is true whether using the mean or the median.

Bahcall et al. (1997) classify four of their hosts as spirals, 12 as ellipticals, and the remaining four as interacting or of indeterminate morphology. Ignoring the interacting and indeterminate types, we agree with their morphology classifications, with the possible exceptions of PG 1116+215 and PG 1444+407. Bahcall et al. (1997) classify both of these as

---

[6] Available at ftp://www.astro.yale.edu/pub/sabbey/thesis.ps.gz.

elliptical, but we find that they are disklike. In our analysis, they are best fitted by exponential profiles, and they contain central bulges, although neither host shows visual evidence of spiral arms. One of the central conclusions of Bahcall et al. (1997), that elliptical galaxies can host either radio-loud or radio-quiet QSOs, is confirmed by our study. Finally, we agree with their finding that the host magnitude distribution is inconsistent with a Schechter (1976) function.

The sample of McLure et al. (1999) includes 15 QSOs with a redshift range of $0.1 \leq z \leq 0.35$. Transforming their results into M_V, using $V-R = 0.7$ for ellipticals and $V-R = 0.6$ for spirals (Fukugita et al. 1995), we find that their host luminosity distribution is narrower ($-21.9 > M_V > -23.6$) than ours, although with the peak in the same magnitude bin ($M_V \sim -23$) as ours. They find only two QSOs with spiral hosts (with the remaining 13 being ellipticals), while we have a much larger fraction of spirals, 26/70. But note that we classify Mrk 1014 as a spiral on the basis of its arms, while they list it as an elliptical on the basis of its $r^{1/4}$ law radial profile. While McLure et al. (1999) find that essentially all radio-quiet QSOs with nuclear luminosities $M_V < -23.7$ ($M_R < -24.0$) have elliptical hosts, we find several spiral hosts with nuclei in this luminosity range. However, our data do show that the radio-quiet QSOs with the brightest nuclei reside in elliptical hosts, while those with the dimmest nuclei reside in spiral hosts. This may still lend support to their idea that the correlation between black hole and bulge mass derived by Magorrian et al. (1998) affects the distribution of nuclear luminosities between elliptical and spiral hosts.

Since this investigation uses archival *HST* images, we also compare our host apparent filter magnitudes, m_{host}, against those of the above two studies, for cases in which we use the same images. This allows a comparison of the measurement techniques themselves. For the Bahcall data, this corresponds to 16 objects from *HST* observing programs 5099, 5343, and 5849 (see Table 1 for the object names). For the McLure data, this corresponds to 11 objects from program 6776 (but note that PKS 2135−147 is not included in their paper). We note in particular that Bahcall et al. (1997) provide the results of both their one-dimensional and two-dimensional model fits; while they adopt the two-dimensional magnitudes in their analysis, we find that their one-dimensional magnitudes agree better with ours and thus adopt their one-dimensional magnitudes in the following comparison. There are 27 other objects for which there exist published m_{host}-values taken from the same observations we use. These include the nine objects observed by Boyle (program 6361) and published in Schade, Boyle, & Letawsky (2000), the 10 observed by Impey (program 5450) and published in Hooper, Impey, & Foltz (1997), the four observed by Disney (program 6303) and published in Boyce et al. (1998) (note that we exclude PG 0043+039, for which the published host measurements are very uncertain, and IR 0450−2958 and IR 0759+6508, which are published in Boyce et al. 1996 without values for m_{host}), the two observed by Hutchings (program 5178) and published in Hutchings & Morris (1995), and the two observed by Macchetto (program 5143) and published in Disney et al. (1995) and Boyce et al. (1998).

The comparisons show that the one-dimensional m_{host} data of Bahcall et al. (1997) are on average 0.09 ± 0.35 mag fainter than ours, and the m_{host} data of McLure et al. (1999) are an average of 0.16 ± 0.33 mag fainter than ours. Look-ing at all 54 objects together, we find that published m_{host} results average 0.30 ± 0.62 mag fainter than ours. Although there is considerable scatter to these differences in apparent filter magnitudes, we believe that at least part of the difference may be systematic and lie in our direct measurement of the apparent host magnitude from the PSF-subtracted image, without relying on a simple galaxy model except at large radii. In theory, if the host model fit is weighted inversely to the square of the Poisson noise in the image ($1/\sigma$), the model's magnitude will be slightly fainter than that of the actual host image. In practice, we find that our host models are ≈ 0.25 mag fainter than the host magnitudes we calculate in § 3.3. The host magnitudes we adopt (§ 3.3) are not affected much by this bias in the models.

6. CONCLUSIONS

1. We have assembled a sample of 71 *HST* WFPC2 imaging observations of luminous QSOs (total nuclear plus host light $M_V \leq -23$ in our adopted cosmology with $H_0 = 50$ km s^{-1} Mpc^{-1}, $q_0 = 0.5$, and $\Lambda = 0$) in the redshift interval $0.06 \leq z \leq 0.46$. We derive results on QSO host and nuclear luminosities and on host morphology, using procedures we have developed, and we compile results on radio loudness. Of the 71 QSOs, we detect hosts in 70 cases. The one nondetection may be due to filter choice (F336W) and faintness.

2. The host galaxies span a narrow range of luminosities and are exceptionally bright, much more so than normal galaxies, usually $L > L_V^*$.

3. The hosts are almost equally divided between subclasses of radio-loud QSOs with elliptical hosts (22 objects), radio-quiet QSOs with elliptical hosts (22 objects), and radio-quiet QSOs with spiral hosts (21 objects). Radio-loud QSOs with spiral hosts (at most four objects) are extremely rare.

4. The elliptical host luminosity distribution of the radio-loud QSOs differs significantly from both the elliptical and spiral host luminosity distributions of the radio-quiet QSOs. However, the latter two distributions are more compatible. Spiral hosts are typically nearly as luminous as elliptical hosts, and the hosts of radio-loud QSOs are typically 0.5 mag brighter than those of radio-quiet QSOs.

5. Using a weighting procedure, we derive the combined luminosity function of low-redshift QSO host galaxies. Subject to systematic uncertainties in normalization procedures, the luminosity function of nearby QSO hosts peaks near the point at which the normal galaxy luminosity function falls off. We conclude that the host luminosity function of low-redshift QSOs differs in shape from the normal galaxy luminosity function but that they coincide at the highest luminosities. With a QSO defined in historically traditional terms, i.e., the total nuclear plus host light has $M_V \leq -23$, the ratio of the number of nearby QSO hosts to the number of normal galaxies is $\mathscr{R} = \left(L_V/11.48 L_V^* \right)^{2.46}$, where L_V^* corresponds to $M_V^* = -22.35$. This ratio represents an empirical parameterization of the probability that a galaxy with luminosity L_V will host a QSO at redshift $z \approx 0.26$.

REFERENCES

Bahcall, J. N., Kirhakos, S., Saxe, D. H., & Schneider, D. P. 1997, ApJ, 479, 642

Biretta, J. A., et al. 1995, Wide Field and Planetary Camera 2 Instrument Handbook, Version 3.0 (Baltimore: STScI)

Blanton, M. R., et al. (SDSS Collaboration) 2001, AJ, 121, 2358

Boroson, T. A., Persson, S. E., & Oke, J. B. 1985, ApJ, 293, 120

Boyce, P. J., et al. 1996, ApJ, 473, 760

———. 1998, MNRAS, 298, 121

Boyle, B. J., Shanks, T., Croom, S. M., Smith, R. J., Miller, L., Loaring, N., & Heymans, C. 2000, MNRAS, 317, 1014

Brinkmann, W., Yuan, W., & Siebert, J. 1997, A&A, 319, 413

Cristiani, S., & Vio, R. 1990, A&A, 227, 385

de Vries, W. H., O'Dea, C. P., Baum, S. A., & Barthel, P. D. 1999, ApJ, 526, 27

Disney, M. J., et al. 1995, Nature, 376, 150

Dunlop, J. S., Taylor, G. L., Hughes, D. H., & Robson, E. I. 1993, MNRAS, 264, 455

Fukugita, M., Shimasaku, K., & Ichikawa, T. 1995, PASP, 107, 945

Gavazzi, G., Catinella, B., Carrasco, L., Boselli, A., & Contursi, A. 1998, AJ, 115, 1745

Hamabe, M., & Kormendy, J. 1987, in IAU Symp. 127, Structure and Dynamics of Elliptical Galaxies, ed. T. de Zeeuw (Dordrecht: Reidel), 379

Hooper, E. J., Impey, C. D., & Foltz, C. B. 1997, ApJ, 480, L95

Hooper, E. J., Impey, C. D., Foltz, C. B., & Hewett, P. C. 1995, ApJ, 445, 62

———. 1996, ApJ, 473, 746

Hutchings, J. B., Crampton, D., & Campbell, B. 1984, ApJ, 280, 41

Hutchings, J. B., & Morris, S. C. 1995, AJ, 109, 1541

Kellermann, K. I., Sramek, R., Schmidt, M., Shaffer, D. B., & Green, R. 1989, AJ, 98, 1195

Krist, J., & Burrows, C. J. 1995, Appl. Opt., 34, 4951

Krist, J., & Hook, R. 2001, The Tiny Tim User's Guide (Baltimore: STScI)

Kristian, J. 1973, ApJ, 179, L61

Kukula, M. J., Dunlop, J. S., McLure, R. J., Miller, L., Percival, W. J., Baum, S. A., & O'Dea, C. P. 2001, MNRAS, 326, 1533

Lehnert, M. D., van Breugel, W. J. M., Heckman, T. M., & Miley, G. K. 1999, ApJS, 124, 11

Magorrian, J., et al. 1998, AJ, 115, 2285

Malkan, M. A., Margon, B., & Chanan, G. A. 1984, ApJ, 280, 66

McLeod, K. K., & Rieke, G. H. 1994a, ApJ, 420, 58

———. 1994b, ApJ, 431, 137

McLure, R. J., Kukula, M. J., Dunlop, J. S., Baum, S. A., O'Dea, C. P., & Hughes, D. H. 1999, MNRAS, 308, 377

Metcalfe, N., Ratcliffe, A., Shanks, T., & Fong, R. 1998, MNRAS, 294, 147

Nolan, L. A., Dunlop, J. S., Kukula, M. J., Hughes, D. H., Boroson, T., & Jimenez, R. 2001, MNRAS, 323, 308

Pence, W. 1976, ApJ, 203, 39

Postman, M., & Lauer, T. R. 1995, ApJ, 440, 28

Remy, M., Surdej, J., Baggett, S., & Wiggs, M. 1997, in 1997 *HST* Calibration Workshop, ed. S. Casertano, R. Jedrzejewski, C. D. Keyes, & M. Stevens (Baltimore: STScI), 374

Sabbey, C. N. 1999, Ph.D. thesis, Yale Univ.

Schade, D. J., Boyle, B. J., & Letawsky, M. 2000, MNRAS, 315, 498

Schechter, P. L. 1976, ApJ, 203, 297

Schlegel, D. J., Finkbeiner, D. P., & Davis, M. 1998, ApJ, 500, 525

Smith, E. P., Heckman, T. M., Bothun, G. D., Romanishin, W., & Balick, B. 1986, ApJ, 306, 64

Stockton, A., & MacKenty, J. W. 1987, ApJ, 316, 584

Surdej, J., Baggett, S., Remy, M., & Wiggs, M. 1997, in 1997 *HST* Calibration Workshop, ed. S. Casertano, R. Jedrzejewski, C. D. Keyes, & M. Stevens (Baltimore: STScI), 386

Véron-Cetty, M. P., & Véron, P. 1998, A Catalogue of Quasars and Active Galactic Nuclei (8th ed.; Garching: ESO)

Voit, M., ed. 1997, *HST* Data Handbook, Version 3.0, Vol. 1 (Baltimore: STScI)

Yuan, W., Brinkmann, W., Siebert, J., & Voges, W. 1998, A&A, 330, 108